To access the final edited and published work see http://dx.doi.org /10.1039/ B914950C

Metal surface nucleated supercritical fluid–solid–solid growth of Si and Ge/SiOx core–shell nanowires

Christopher A Barrett[†], *Robert D Gunning*[†], *Thomas Hantschel*[‡], *Kai Arstila*[‡] *and Kevin M Ryan*[†*]

Materials and Surface Science Institute and Department of Chemical and Environmental Sciences,

University of Limerick, Limerick, Ireland and Interuniversitair Micro-Elektronica Centrum, Kapeldreef 75 B-3001, Leuven, Belgium

RECEIVED DATE (to be automatically inserted after your manuscript is accepted if required according to the journal that you are submitting your paper to)

*To whom correspondence should be addressed. Email: Kevin.M.Ryan@ul.ie

[†] Materials and Surface Science Institute and Department of Chemical and Environmental Sciences, University of Limerick.

[‡] Interuniversitair Micro-Elektronica Centrum.

High yields of single-crystalline silicon nanowires and germanium/silicon oxide core-shell nanostructures were synthesized using a supercritical fluid-solid-solid growth mechanism. The formation of the one-dimensional nanostructures was investigated on stainless steel and titanium reactor cell walls. The nanowire growth is diffusion controlled with no catalyst particles being observed at the tip of the nanowires, which is contrary to the characteristic feature of a one-dimensional growth based on the vapor-liquid-solid mechanism. The diameter and length of the nanowires were in the ranges of 30-60 nm and 1-10 μm, respectively, as found by high-resolution electron microscopy. The nanowires

were characterized by transmission electron microscopy (TEM), energy-dispersive X-ray spectroscopy (EDX) and scanning electron microscopy (SEM).

Christopher A Barrett[†], Robert D Gunning[†], Thomas Hantschel[‡], Kai Arstila[‡] and Kevin M Ryan[†*]

J. Phys. Chem. C

Synthesis of Silicon and Ge-Core/SiO_x-Shell Nanowires from Metal Surfaces by Supercritical Fluid-Solid-Solid Growth

High yields of single-crystalline silicon nanowires and germanium/silicon oxide core-shell nanostructures were synthesized using a supercritical fluid-solid-solid growth mechanism. The formation of the one-dimensional nanostructures was investigated on stainless steel and titanium reactor cell walls. The nanowire growth is diffusion controlled with no catalyst particles being observed at the tip of the nanowires, which is contrary to the characteristic feature of a one-dimensional growth based on the vapor-liquid-solid mechanism.

I. Introduction

One-dimensional nanostructures, such as semiconductor nanowires, are attracting significant attention for their potential applications in nanoelectronic and photonic devices.[1,2] This is due in part to the ever increasing problem of electromigration and subthreshold leakage in the miniaturization of electronic components for modern information industries. Nanowires offer thermodynamically stable features and are typically defect-free and single-crystalline and thus have a number of advantages over thin films with respect to high-performance one-dimensional arrays of transistors.[3] As some of the most important semiconducting materials, Si and Ge nanowires have also attracted a wide interest due to their unique size dependent electronic and optical properties[4,5] and have been successfully implemented in high capacity power cells,[6,7] field effect transistors[8,9] and third generation solar cells.[10,11] The more complex, core-shell nanowires of Ge/SiO_x have drawn considerable interest given the higher intrinsic carrier mobilities of Ge, making it the more suitable material for a carrier channel and using Si as the shell material, which simplifies the chemical passivation of the structure, with SiO_x being a much more stable and higher quality surface passivation than Ge oxides.[12,13] Si and Ge nanowires have been prepared by employing a variety of different techniques, such as laser ablation,[14] physical thermal evaporation,[15] chemical vapor deposition,[16,17] and the more popular, vapor-liquid-solid (VLS).[18-20] The widely used VLS growth mechanism provides direct control of nanowire diameter and length and can be applied to a variety of materials including single and compound semiconductors from the group IV, III–V, and II–VI systems.[21,22] Variations of VLS have been developed to realize anisotropic growth in solution (SLS)[23] and in supercritical fluids (SFLS).[24] The application of these methods in realizing one-dimensional (1D) nanostructures is considered to be highly promising for scalable, economical, and controllable growth of a variety of elemental and compound 1D nanocrystals.[25] One of the greater focuses of this area is that of Si and Ge nanowires synthesis given their high compatibility with standard CMOS technology and their expected ease of integration in future electronic devices.[26] To realize group IV nanowire based electronic devices, it is important to gain precise control of their length, diameter, purity and structural quality. Of these, one of the most crucial problems has been nanowire purity due to the contamination

occurred through the use of metal seed catalysts in the VLS technique.[27] In general, Si and Ge nanowires are most commonly grown using a vapor-liquid-solid process employing heavy metals such as Au, Bi, Co, Cu, Ni, and Fe as catalysts.[23,28,29] Gold is the most widely used catalyst for silicon nanowire growth because of its simple eutectic-type phase diagram and low eutectic temperature (360°C). However, Au is also known to diffuse very rapidly into silicon and makes deep centers that increase p-n junction leakage and decrease dielectric strength.[30,31] It has been reported that metal from the catalyst particle wets the nanowire sidewalls, causing a tapering of the nanowire diameter and eventually consuming the droplet and terminating VLS growth.[32] One answer to these issues has been the use of the vapor-solid-solid (VSS) technique. Growth in this manner occurs in a similar fashion to that of VLS growth, however the mechanism proceeds at temperatures below the required melting points of the bulk eutectic alloy.[33] As a result a solid phase catalyst particle provides the preferential interface for the diffusion of monomer into the growing crystal. The incorporation of unintentional impurities, particularly from the metal catalyst, may be reduced in VSS nanowires due to the reduction in atom diffusivity and solid solubility associated with nanowire growth at lower temperatures. Also, particle ripening by diffusion could be mitigated if solid metal catalysts are used, particularly at lower temperatures, which will help maintain narrower diameter distributions.

Here we demonstrate the first reported method of seedless, supercritical fluid-solid-solid (SFSS) growth of single-crystal Si and Ge/SiO_x one-dimensional nanostructures from the thermolysis of a metal-organic precursor in a supercritical fluid medium of CO_2. The nanowires could be formed in high yields on the side walls of stainless steel and titanium high pressure reaction cells, without the use of structure directing metal seeds. Higher concentrations of precursor could be suspended in the fluid through the addition of trioctylphosphine, a coordinating ligand. Utilizing the high temperatures and diffusivity rates attributed by supercritical CO_2, rapid precursor thermolysis and monomer supply drive the fast saturation needed for the solid-state diffusion growth process. The electrical characteristics of individual nanowires grown from these metal surfaces, is investigated by means of mechanical nanoprobing. The method differs from the commonly used vapor-liquid-solid mechanism, where the

utilization of a liquid alloy droplet acts as a growth template and is commonly observed at the tip of growing nanowires.

II. Experimental Section

All chemicals were used as received unless otherwise stated. Diphenylsilane (97%) and Trioctylphosphine (>90%) used was received from Sigma-Aldrich and Diphenylgermane (95%) was supplied by Gelest, all of which was stored and dispensed from a nitrogen filled glove box. Experiments were conducted using Liquid Carbon Dioxide from BOC (99.85%) and the reaction cells, stainless steel tubing and connections were all supplied from High Pressure Equipment Co. The micro reactors used were of a grade-2 titanium and 316 stainless steel construction, designed specifically for high temperatures and pressures. A Teledyne Model 260D Computer Controlled Syringe Pump was used to pressurize the system and an Applied Test Systems Inc. Model 3210, 3-zone heating furnace, was used to regulate temperature.

Nanowires were synthesized by thermal decomposition of diphenylgermane (DPG) and diphenylsilane (DPS) in the presence of trioctylphosphine (TOP), at 650°C and 4000 psi in supercritical carbon dioxide (sc-CO_2). The reactions were carried out in 5 ml, high pressure, stainless steel or titanium reaction cells. In a typical synthesis of silicon nanowires, a stainless steel react ion cell was loaded with 400 µl of TOP and 500 µl of DPS under an inert atmosphere of a nitrogen filled glove box. For the synthesis of Ge/SiO_x core-shell nanowires, 400 µl of TOP, 250 µl of DPS and 250 µl of DPG were loaded into a titanium reaction cell. All cells were sealed under nitrogen and then removed from the glovebox where they were then connected to the computer controlled syringe pump using ⅛ inch stainless steel high pressure tubing. Using the syringe pump, liquid CO_2 was pumped into a reaction cell and the pressure was increased above its critical point (T_c = 31°C, P_c = 1030 psi), to 3000 psi. The 3-zone heating furnace was preheated to 665°C, 15°C above the required reaction temperature of 650°C. At this point the reactor was placed in the furnace and would reach the desired temperature in under a

minute. When the system had stabilized at the desired temperature, the pressure was further increased to 4000 psi. Both temperature and pressure were then kept constant for the proceeding reaction time of 3 hours, at which point the furnace was opened and cooled to room temperature. CO_2 was then vented from the reaction cell leaving a black powder residue.

Chloroform was injected into the cell and subsequently removed to extract the nanowires from the reactor. All samples were initially centrifuged at 4000 rpm for 10 minutes to remove a precipitate, containing carbon by-products of the reaction. The nanowires were then precipitated by adding 5-10 ml of acetone and centrifuging at 5000 rpm for 10 minutes. The remaining solution was discarded and the precipitate was re-dispersed with 5 ml of chloroform. These steps were repeated twice more before the precipitate was again re-dispersed in 10 ml of chloroform for analysis. All samples were sealed in glass vials which were stored in a nitrogen filled glove box to prevent against nanocrystal oxidation.

The transmission electron microscopy (TEM) images of samples and the corresponding selected area electron diffraction (SAED) patterns were taken on a JEOL JEM-2011 electron microscope operated at an accelerating voltage of 200 kV using a LaB6 filament. Energy dispersive X-ray (EDX) analysis was performed with a Princeton Gamma Tech Prism 1G system with a 10 mm^2 silicon detector and an INCAPentaFET-x3, with a Si(Li) detector and a 30 mm^2 detecting crystal. X-ray diffractograms were recorded on a Philips X'Pert PRO MPD (multi-purpose x-ray diffractometer), using a Cu-Kα radiation source and standard scintillation detector. The scanning electron microscopy (SEM) images of the as-synthesized samples were obtained by a Hitachi S-4800 and a Philips XL-30 high resolution scanning electron microscope operated at 5 kV. Electrical transport measurements were performed in the ultrahigh vacuum (UHV) of a Philips XL-30 high resolution scanning electron microscope, allowing the positioning of independent probe tips with nanometer accuracy on individual nanowires while observing the process by scanning electron microscope (SEM). The probes were electrochemically sharpened tungsten wires mounted on and manipulated by piezoelectric actuator elements. Current–voltage (I –V)

curves were measured with the nanowires held at room temperature, using a programmable semiconductor test system (Keithley, model 4200SCS).

III. Results and Discussion

Figure 1 shows an SEM image of the silicon product, grown from stainless steel reactors, where yields of ~30 mg of nanocrystalline product were obtained in large bundles of nanowires. The silicon nanowires were found to aggregate into large bundles, which settled out of solution after an hour, but could be readily redispersed by light sonication. No visible luminescence was apparent from the chloroform dispersions of the nanowires, which would be expected given that the average diameter of the nanowires observed was larger than the Bohr excitation radius for Si (r = 4.9 nm). Following the centrifugation and redispersion cleaning steps, the nanowires collected were relatively clean with no significant by-product observable. However, SEM analysis did reveal small dark regions of an organic nature, scattered across the sample which, upon close inspection, decomposed under the intensity of the beam. It is likely that residual surfactant of TOP and its oxide form, trioctylphosphine oxide would be still present in the sample and can be attributed to these organic areas. Observations from SEM analysis of the silicon product, found predominantly straight, crystalline nanowires, with diameters typically ranging between 10 and 50 nm and lengths greater than 1 μm.

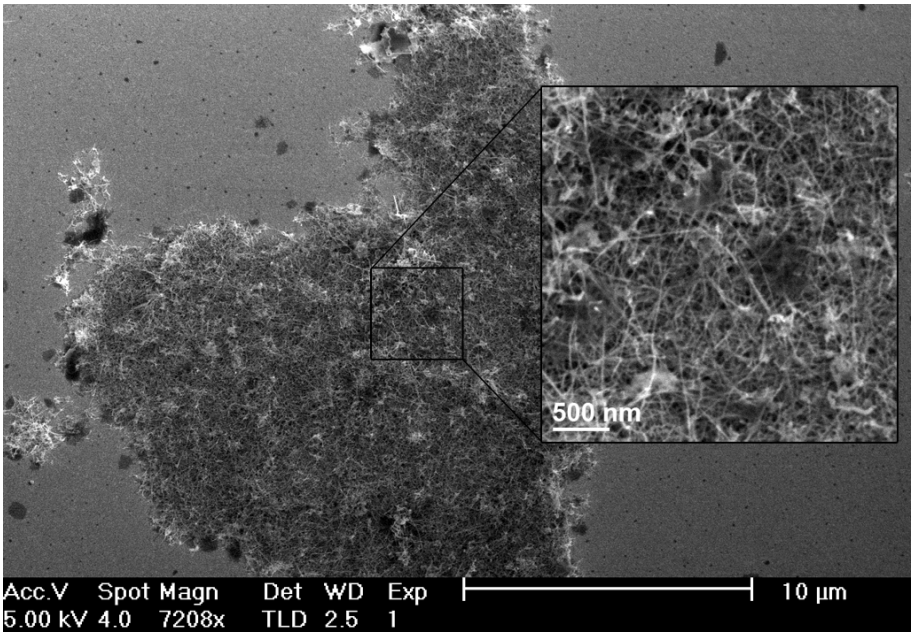

Fig. 1 SEM image from high density areas of silicon nanowires collected from a stainless steel reaction vessel.

Supercritical fluids are unique in that they can diffuse through solids like a gas, and dissolve materials like a liquid. In the context of this setup, it is expected that the supercritical fluid, CO_2, acts both to thermally decompose the phenyl precursors but also, given its high diffusivity rate, maintains a constant high concentration of monomer supply to nucleation sites. Small fluctuations in pressure or temperature, close to the critical point, can result in large changes in the density of a supercritical fluid, allowing many of its properties to be "tuned". For this reason, an investigation with pressure changes of ±1000 psi from the optimum conditions were conducted but no large degree of effect on the nanocrystals yield was found. However, lowering reaction temperatures did reduce the overall yield in both cases, which in turn increased the amount of amorphous by-product formed. Decomposition of the supercritical CO_2 occurred readily at elevated reaction temperatures (>700°C), which stifled the growth of any crystalline material. It was noted that in the absence of TOP from the system, Si nanowire growth did not occur. Previous studies have shown that the addition of hydrocarbon ligands to sc-CO_2 not only act as capping ligand for the subsequent nanocrystals formed but also attributes a degree of steric stabilization to emerging nuclei during the reaction, playing a crucial role to anisotropic growth.[34,35] Supercritical CO_2

is also known to have a low degree of solvation but through the addition of TOP, the initial precursor concentrations in the fluid solution could be raised.

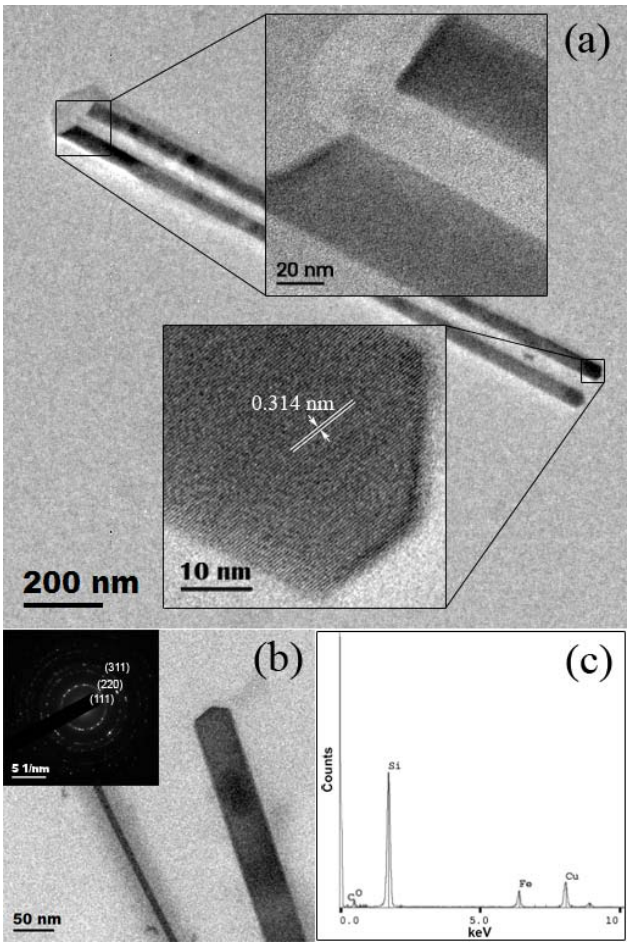

Fig. 2 TEM image (a) of Si nanowires with the corresponding HRTEM images, taken from either ends of the nanowires, inset. HRTEM image (b) of a Si nanowire, with the corresponding single crystal diffraction pattern inset. An EDX spectrum obtained from the spectroscopic analysis of the Si nanowires (c).

Dilute dispersions of the nanowires in toluene were drop cast on to carbon coated copper grids for TEM analysis. The yields obtained from the synthesis with DPS and TOP in steel reactors was comprised of pure single crystal nanowires. Figure 2(a) shows a TEM image of two as synthesized Si nanowires that are approximately 1.5 μm in length and 45 nm in diameter. The HRTEM image from the tip of one of the Si nanowires (inset) shows visible lattice fringes from a highly crystalline structure with interplanar spacings of 0.314 nm. This is in good agreement with the d spacing of the (111) plane

for diamond cubic crystalline silicon. One general but very noticeable feature observed from TEM was that the bases of the nanowires were found to be flat however the opposite ends were usually more geometrically defined owing to a crystal faceting of the nanowire tips. The faceted ends of the nanowires would seem to point towards solution born nanocrystals however the base of the nanowires, being found to be flat, is more suggestive of the nanowires being nucleated and grown from a surface rather than in solution. The flat ends of the nanowires may be attributed to a fracturing of the nanocrystal along a crystallographic plane during removal from the cell walls. Nanowire diameter sizes were found to typically vary in measure, evidence of which can be seen in figure 2(b) where two nanowires of 11 and 46 nm in diameter are shown. The corresponding electron diffraction analysis (inset) of the area observed in figure 2(b), gave a polycrystalline diffraction pattern, from which the maximum intensity of the diffraction rings gave d spacings of 0.313, 0.191, and 0.162 nm. These spacings can be matched to the lattice parameters of (111), (220) and (311) for the diamond cubic crystal structure of silicon. EDX analysis from an area of high nanowire concentration is shown in figure 2(c). An expected strong Si peak was observed with lower intensity peaks of O, C, Fe, and Cu also indicated. The copper and carbon peaks originated from the copper TEM grid and its amorphous carbon film support, while the minor oxygen peak can be contributed to native oxide formation along the silicon nanowires. With no metal catalyst particles being added to the synthesis of the Si nanowires it can be assumed that the Fe detected in the nanowires is indicative that nucleation occurred from the side walls of the reactor given that this is the only source of Fe during the synthesis.

Furthering the study of silicon nanowire growth from metal surfaces, a move from stainless steel to titanium reactor vessels was made, with all other reaction parameters be kept as before. However in the subsequent investigations with the Ti high pressure cells, it was discovered that side wall nucleation of Si nanowires did not occur under the same conditions. It is thought that higher temperatures would be necessary for anisotropic growth of crystalline silicon to occur from Ti, which in this case, was found to be beyond the scope of the temperatures attainable with supercritical CO_2. To overcome this barrier, a mixture of silicon and germanium precursors were used in the reaction so that an alloy of the two would

reduce the required nucleation temperature. Ge offers the advantage of similar chemical properties to those of Si, as well as weaker binding energies, allowing crystal growth at much lower temperatures. Through the addition of DPG to the reaction system, in a 1:1 ratio with DPS, one-dimensional growth of the more novel, core-shell nanostructures was made possible. At equivalent reaction temperatures and pressures, Ge/SiO_x core-shell nanowires (figure 3) of similar quality were identified. By comparison, Ge/SiO_x core-shell nanostructures, grown from titanium reaction cells, were produced in slightly higher yields of ~40 mg. This can be contributed to the lower temperatures required for nanocrystalline germanium to be nucleated, leaving a smaller percentage of amorphous by-products to be removed. Figure 3 shows a typical bundle of core-shell nanostructures where larger amounts of TOPO can be seen amongst the nanowires. The inset indicates the degree of passivation from the surfactant, which is formed from the oxidation of TOP during synthesis and was found to nanowire solubility in toluene.

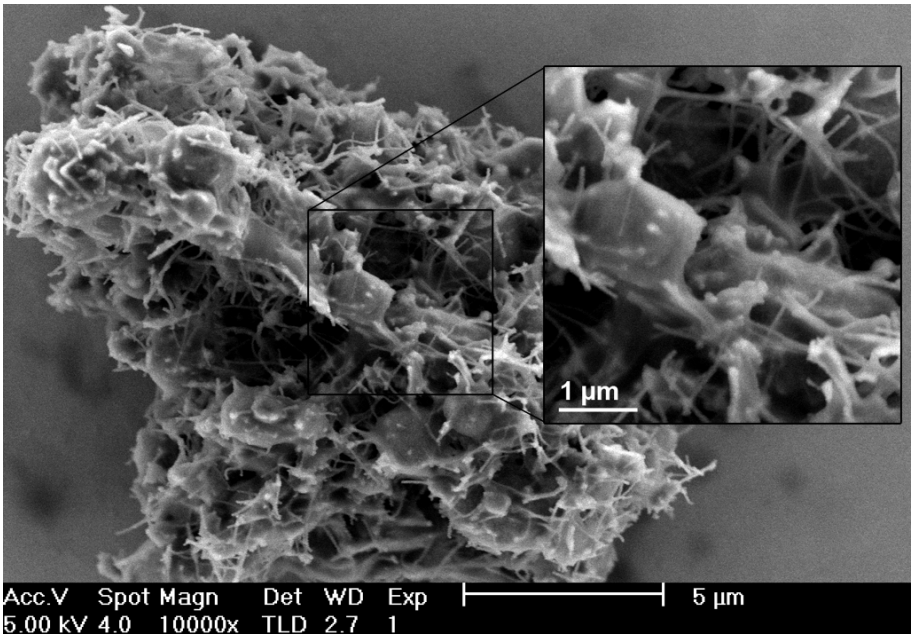

Fig. 3 SEM image from high density areas of Ge/SiO_x core-shell nanowires collected from a titanium reactor.

In figure 4(a), a crystalline germanium core is clearly visible, surrounded by a thick layer of amorphous SiO_x. Decomposition of DPG occurs at lower temperatures to that of DPS, allowing the formation of Ge nanowires to occur initially, with subsequent encapsulation from the deposition of

amorphous SiO_x occurring there after. The corresponding selected area electron diffraction (figure 4(b)), indicates that the core is pure single crystal germanium. The indexed Bragg reflections for this core-shell nanowire correspond to the [1-12] zone axis. Calculations for the rectangular pattern give a spacing of 0.314 and 0.192 nm respectively, which can be indexed for the (-111) and (220) directions of diamond cubic germanium with interplanar angles of 90°. Analysis from several nanowires found that growth occurred predominantly in the [110] direction with a smaller percentage of nanowires growing in the [111] direction. EDX analysis taken over a wide area (figure 4(c)), shows a strong signal from the SiO_x shell enclosing the nanowire with a lower intensity peak emerging from the Ge core. It is expected that the degradation of TOP, added as a capping ligand for the nanowires, may cause a degree of doping in the semiconducting nanowires. Evidence of which can be seen in the weak signal picked up from the presence of phosphorous in the sample.

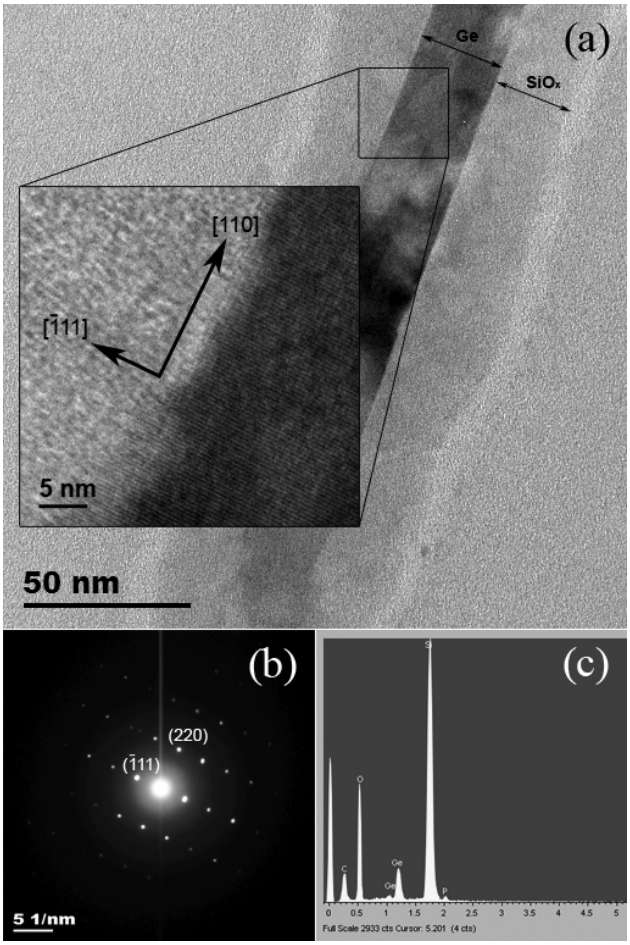

Fig. 4 TEM image (a) of Ge/SiO_x core-shell nanowires with the corresponding HRTEM images, taken from either ends of the nanowires, inset. HRTEM image (b) of a Si nanowire, with the corresponding single crystal diffraction pattern inset. An EDX spectrum obtain from the spectroscopic analysis of the Si nanowires (c).

Figure 5(a) shows a typical core-shell nanowire grown from a Ti substrate (placed inside a reactor vessel during synthesis) and an approaching tungsten tip, which was used to mechanically sever the nanowire. The roots left behind after removal of a core-shell nanowire (figure 5(b)) show cross sections where the conductive Ge core can be found in the centre. From SEM analysis, it was apparent that the nanowires were randomly nucleating from the surface of the titanium substrate. Nanowires were picked and placed onto carbon coated TEM grids, using a Kleindiek nanomanipulator. The high angle angular dark field TEM image, shown in figure 5(c), gives a clear profile of a typical core-shell nanowire with a Ge crystalline core of 35 nm in diameter. At first it was thought that Ti contamination in the nanocrystalline yield was very small and was not detected at low resolution analysis. However, a more extensive examination from the base of the core-shell nanowires found trace elements of the metal. The EDX spectra obtain (figure 5(d,e)), are taken from a line profile analysis of the Ge/SiO_x nanowire, where a large degree of phosphorous doping can be seen in the nanowire. The presence of Ti is clearly visible, however from the positional analysis, the Ti contamination appears to be localized to the Ge core.

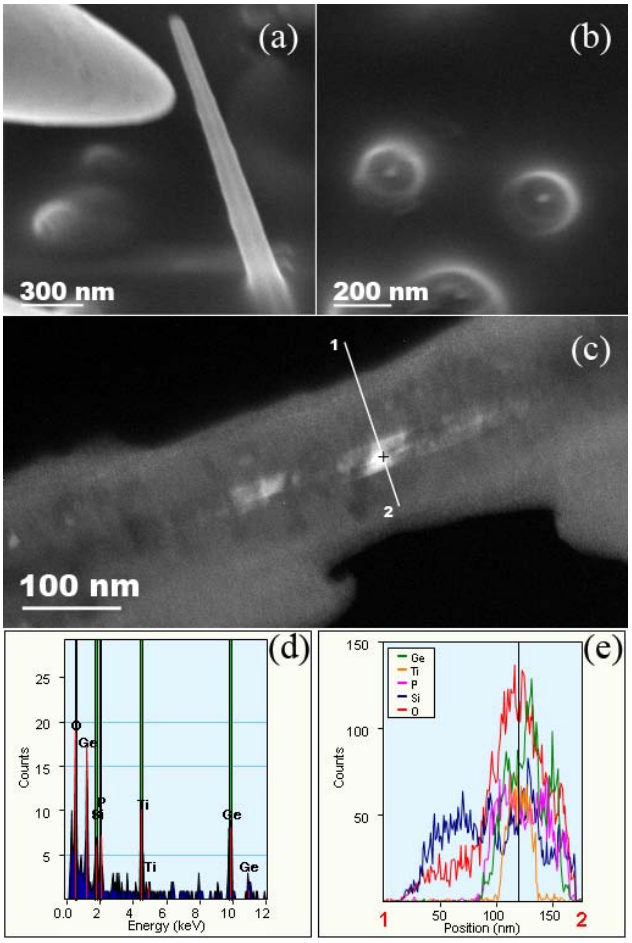

Fig. 5 SEM image (a) of a Ge/SiO_x core-shell nanowire being picked by a nanomanipulator and (b) cross-sectional image of the roots left behind. High angle angular dark field TEM image (c), showing a side profile of a picked core-shell nanowire. EDX spectra obtain from the line profile analysis of the Ge/SiO_x nanowire (d,e).

Nanowires were deposited from solution on to a silicon wafer, where individual nanowires could be extracted from bundles for electrical characterization. Core-shell nanowires were plucked by maneuvering a tungsten probe to form a contact with the nanostructure, which was subsequently reinforced using localized carbon deposition (figure 6(a)). This carbon adhesion between tungsten probe and nanowire afforded a bond, strong enough to retract the probe along with the desired nanowire (figure 6(b)). A second probe could then be maneuvered into position at the opposite end of the nanowire to complete the circuit for transmission line analysis of current, measured by a picoammeter. In the electrical characterization experiments, a circuit was configured so that a potential difference

could be applied between the tungsten probes connected at either end of a specific nanowire. The current–voltage sweep plotted in figure 6(c) are measurements taken across a Ge/SiO_x nanowire separated by 2.5 μm (inset) and show non-linear transport. It is most likely that the core-shell nanowire suspended across the two probes can only make a physical contact with the SiO_x shell. This insulating barrier forms an obstacle in the characterization, causing the SiO_x shell to dominate the electrical characteristics. The non-linear transport properties observed indicate an expected tunneling affect through the amorphous shell. Using a Brinkmann fit the insulating barrier was calculated at 55 nm, which is consistent with the thickness range of 35-60 nm observed for SiO_2.

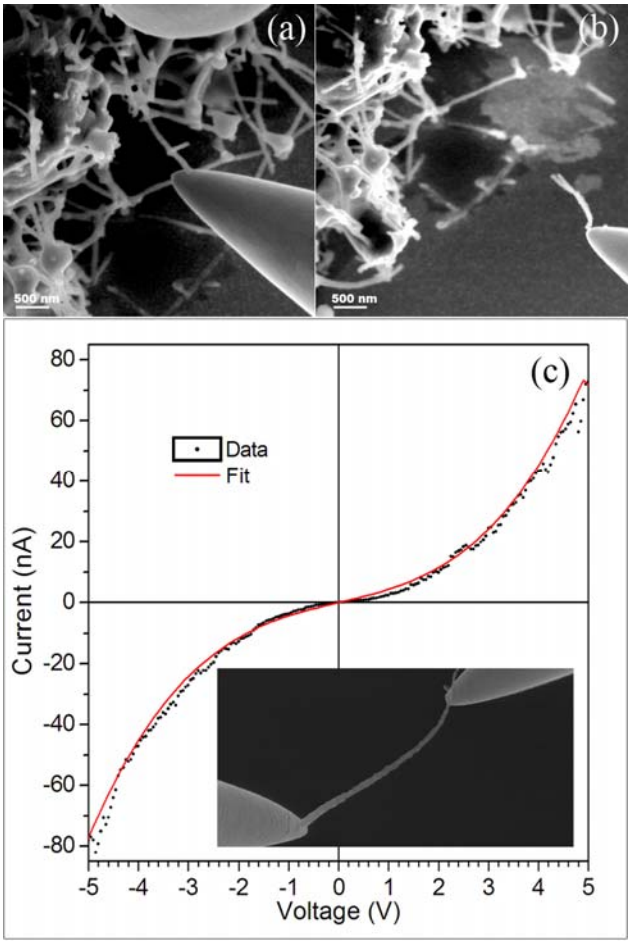

Fig. 6 SEM image (a) of a tungsten tip approaching a Ge/SiO_x nanowire and (b) the subsequent picking of an individual nanowire. Current–voltage graph taken from a Ge/SiO_x nanowire suspend across two tungsten probes during electrical characterization (inset).

It is generally accepted that the catalytic nature of the VLS method, in the case of untapered nanowires, produces long straight nanostructures with a very distinctive metal seed droplet at the tip.[36] However in our case, the nanowires yielded showed no traces of catalytic metal seed particles. In contrast, the nanowires were found to have well faceted tips at one end, while having flat bases at the other end. The faceted ends of the nanowires would seem to point towards solution born nanocrystals which can typically be seen in the synthesis of other nanomaterials, such as II-VI semiconductors.[37] However the base of the nanowires, being found to be flat, is more suggestive of the nanowires being nucleated and grown from the metal sidewalls of the reactor vessels, rather than in solution. The lowest liquid eutectic of Ti and Ge in its bulk, equilibrium phase diagram, occurs at temperatures above 900°C, markedly above the 650°C used here to form Ge/SiO_x nanostructures. Thus it can be concluded that a mechanism other than the VLS method appears to control the nanowire formation.

A solid-state diffusion mechanism, proposed by Kamins et al, described a process of Si diffusion into Ti to form crystalline $TiSi_2$ "nano-islands" at temperatures of ~800°C, which acted as nucleation sites for Si nanowires.[38] Related studies have found that Fe can also be used in the growth of single crystal ZnSe nanowires, where again, a diffusion process on or through the catalyst particle in the solid state is the suggested mechanism, in contrast to the commonly assumed liquid phase growth models.[39] In a similar fashion, pure Fe substrates have been used in the growth of Ge nanowires by means of a CVD process.[40] With the growth temperatures in this study, being well below the bulk eutectic temperatures in each case, a solid seeding mechanism is the most likely route of formation. According to binary phase diagrams of Si-Fe, a high saturation of Si monomer, within the steel reactor and at 650°C, should lead to the formation of an iron silicide epilayer at the fluid-solid phase boundary. It is believed that this thin alloy film acts as a medium for Si, promoting isotropic growth of Si nanowires from the cell walls, by means of the solid state diffusion process (figure 7). In the case of Si nanowire growth from a Ti surface, $TiSi_2$ would be expected to form at temperatures around 600°C, however the subsequent rate of silicon diffusion would be too low for anisotropic growth to occur. As a result one-dimensional nanostructures were not found to form, which fits well with the proposed mechanism of

solid seed diffusion, as the minimum temperatures required for anisotropic growth in a Si-Ti binary system are upwards of 800°C. The maximum temperature range of sc-CO_2 was sufficiently high for Ge diffusion to readily occur in the $TiGe_2$ epilayer formed.

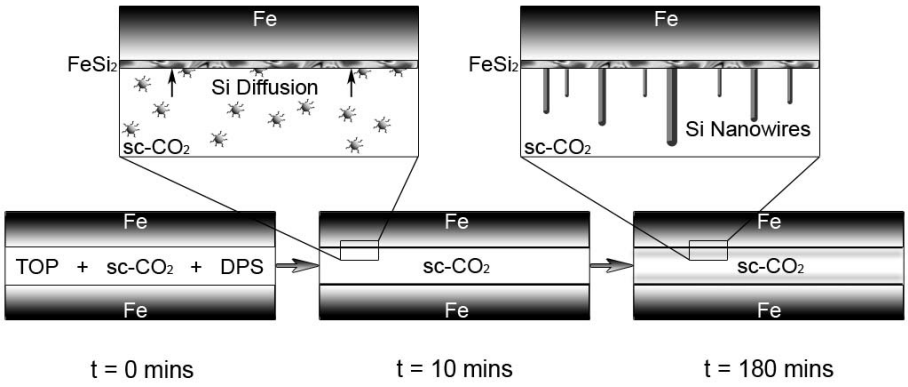

Fig. 7 A schematic showing the stages of surface diffusion in the eventual nucleation of Si nanowires.

The thermolysis of the phenyl-precursors in sc-CO_2 delivers high concentrations of monomer for subsequent diffusion into the metal walls of the reaction vessel. The intermediate transport properties of supercritical fluids allow a faster rate of monomer supply in diffusion limited reactions compared to those of liquid based systems. Its high densities also provide good solvation and thus increases reactant loadings compared to gas-phase systems.[41] At the experimental temperatures used, thin films of Si-Fe and Ge-Ti binary alloys can be formed through surface diffusion. Surface diffusion is a general process involving the motion of atoms or atomic clusters at solid material surfaces. The process can generally be thought of in terms of atoms jumping between adjacent adsorption sites on a surface. Just as in bulk diffusion, this motion is typically a thermally promoted process with rates increasing with increasing temperature. Other systems have been shown to display a diffusion behavior which leads to nano-dimensional isotropic growth from metal surfaces.[40,42] Nano-crystalline domains can arise from this surface diffusion, acting as nucleation sites for isotropic growth.[43,44] Orientational anisotropy takes form according to the difference in both diffusion rates and mechanisms at the various surface features of a given material. Rapid diffusion through crystalline domains of the surface can promote anisotropic nanowire growth from the solid-fluid phase boundary. Close packed crystal lattices such as the fcc

[110], tend to have higher diffusion rates as well as increased electron and hole transport, than the correspondingly more open faces of fcc [100], from the same material.[45] These growth rate variations are reflected in the predominant growth seen for nanowires in the [110] direction. From this, it is believed that a solid seeding mechanism of growth for the nanostructures occurs at the base of the nanowires, where the metal concentrations were found to be at their highest. Solid-phase seeding can probably occur for any semiconductor with a high solubility in the seed metal. However, the growth temperature must be sufficiently high for fast saturation by solid-state diffusion in the epilayer.

IV. Conclusion

Through the formation of a thin film Si/Ge-metal epilayer, at the solid-fluid phase boundary of the reaction cell, nanowire growth was achieved. We demonstrate that monomer diffusion through the epilayer formed, induces nucleation of anisotropic Si or Ge/SiO_x nanostructures. In summary, thermolysis of Si and Ge phenyl precursors in a sc-CO_2 fluid medium generates a fast monomer saturation which drives the diffusion into the reactor sidewalls forming a binary alloy epilayer of metal reactor and monomer. No evidence of a metal seed droplets were ever found at the head of the nanostructures, with growth occurring instead at the base of the nanowires. The solid-state diffusion of monomer, through nano-crystalline domains in the epilayer, nucleates and extrudes nanowires from their base. The synthetic mechanism presented can be described as supercritical fluid-solid-solid growth. It is reasonable to assume that in the growth of group IV semiconductor nanomaterials, side wall nucleation of by-product one dimensional nanostructures can not be ruled out.

Acknowledgement. This work was supported by Science Foundation Ireland (SFI) through the Principal Investigator program, contract No. 06/IN.1/I85. This work was conducted under the framework of the INSPIRE programme, funded by the Irish Government's Programme for Research in Third Level Institutions, Cycle 4, National Development Plan 2007-2013.

(1) Heo, K.; Cho, E.; Yang, J.-E.; Kim, M.-H.; Lee, M.; Lee, B. Y.; Kwon, S. G.; Lee, M.-S.; Jo, M.-H.; Choi, H.-J.; Hyeon, T.; Hong, S. *Nano Lett.* **2008**, *8*, 4523.
(2) Cui, Y.; Lieber, C. M. *Science* **2001**, *291*, 851.
(3) Park, W. I.; Zheng, G.; Jiang, X.; Tian, B.; Lieber, C. M. *Nano Lett.* **2008**, *8*, 3004.
(4) Tutuc, E.; Appenzeller, J.; Reuter, M. C.; Guha, S. *Nano Lett.* **2006**, *6*, 2070.
(5) Hu, L.; Chen, G. *Nano Lett.* **2007**, *7*, 3249.
(6) Chan, C. K.; Peng, H. L.; Liu, G.; McIlwrath, K.; Zhang, X. F.; Huggins, R. A.; Cui, Y. *Nat. Nanotechnol.* **2008**, *3*, 31.
(7) Chan, C. K.; Zhang, X. F.; Cui, Y. *Nano Lett.* **2008**, *8*, 307.
(8) Ho, T.-t.; Wang, Y.; Eichfeld, S.; Lew, K.-K.; Liu, B.; Mohney, S. E.; Redwing, J. M.; Mayer, T. S. *Nano Lett.* **2008**, *8*, 4359.
(9) Xiang, J.; Lu, W.; Hu, Y.; Wu, Y.; Yan, H.; Lieber, C. M. *Nature* **2006**, *441*, 489.
(10) Garnett, E. C.; Yang, P. *J. Am. Chem. Soc.* **2008**, *130*, 9224.
(11) Th Stelzner; M Pietsch; G Andrä; F Falk; E Ose; Christiansen, S. *Nanotechnology* **2008**, *19*, 295203.
(12) Seong, H.-K.; Jeon, E.-K.; Kim, M.-H.; Oh, H.; Lee, J.-O.; Kim, J.-J.; Choi, H.-J. *Nano Lett.* **2008**, *8*, 3656.
(13) Goldthorpe, I. A.; Marshall, A. F.; McIntyre, P. C. *Nano Lett.* **2008**, *8*, 4081.
(14) Wu, Y.; Fan, R.; Yang, P. *Nano Lett.* **2002**, *2*, 83.
(15) Teo, B. K.; Li, C. P.; Sun, X. H.; Wong, N. B.; Lee, S. T. *Inorg. Chem.* **2003**, *42*, 6723.
(16) Clark, T. E.; Nimmatoori, P.; Lew, K. K.; Pan, L.; Redwing, J. M.; Dickey, E. C. *Nano Lett.* **2008**, *8*, 1246.
(17) Hanrath, T.; Korgel, B. A. *J. Am. Chem. Soc.* **2002**, *124*, 1424.
(18) Zhang, X.; Lew, K.-K.; Nimmatoori, P.; Redwing, J. M.; Dickey, E. C. *Nano Lett.* **2007**, *7*, 3241.
(19) Lu, X. M.; Hanrath, T.; Johnston, K. P.; Korgel, B. A. *Nano Lett.* **2003**, *3*, 93.
(20) Woodruff, J. H.; Ratchford, J. B.; Goldthorpe, I. A.; McIntyre, P. C.; Chidsey *Nano Lett.* **2007**, *7*, 1637.
(21) Fan, H. J.; Werner, P.; Zacharias, M. *Small* **2006**, *2*, 700.
(22) Wacaser, B. A.; Dick, K. A.; Johansson, J.; Borgström, M. T.; Deppert, K.; Samuelson, L. *Adv. Mater.* **2009**, *21*, 153.
(23) Heitsch, A. T.; Fanfair, D. D.; Tuan, H. Y.; Korgel, B. A. *J. Am. Chem. Soc.* **2008**, *130*, 5436.
(24) Davidson, F. M.; Wiacek, R.; Korgel, B. A. *Chem. Mater.* **2005**, *17*, 230.
(25) Mohammad, S. N. *Nano Lett.* **2008**, *8*, 1532.
(26) Wu, X.; Kulkarni, J. S.; Collins, G.; Petkov, N.; Almecija, D.; Boland, J. J.; Erts, D.; Holmes, J. D. *Chem. Mater.* **2008**, *20*, 5954.
(27) Allen, J. E.; Hemesath, E. R.; Perea, D. E.; Lensch-Falk, J. L.; Li, Z. Y.; Yin, F.; Gass, M. H.; Wang, P.; Bleloch, A. L.; Palmer, R. E.; Lauhon, L. J. *Nat. Nanotechnol.* **2008**, *3*, 168.
(28) Tuan, H. Y.; Lee, D. C.; Korgel, B. A. *Angew. Chem., Int. Ed.* **2006**, *45*, 5184.
(29) Ahmad, I.; Fay, M.; Xia, Y.; Hou, X.; Kennedy, A.; Zhu, Y. *J. Phys. Chem. C* **2009**, *113*, 1286.
(30) Oh, S. H.; van Benthem, K.; Molina, S. I.; Borisevich, A. Y.; Luo, W. D.; Werner, P.; Zakharov, N. D.; Kurnar, D.; Pantelides, S. T.; Pennycook, S. J. *Nano Lett.* **2008**, *8*, 1016.
(31) Thompson, K.; Flaitz, P. L.; Ronsheim, P.; Larson, D. J.; Kelly, T. F. *Science* **2007**, *317*, 1370.
(32) Bailly, A.; Renault, O.; Barrett, N.; Zagonel, L. F.; Gentile, P.; Pauc, N.; Dhalluin, F.; Baron, T.; Chabli, A.; Cezar, J. C.; Brookes, N. B. *Nano Lett.* **2008**, *8*, 3709.
(33) Kodambaka, S.; Tersoff, J.; Reuter, M. C.; Ross, F. M. *Science* **2007**, *316*, 729.
(34) Shah, P. S.; Husain, S.; Johnston, K. P.; Korgel, B. A. *J. Phys. Chem. B* **2001**, *105*, 9433.
(35) Lu, X. M.; Korgel, B. A.; Johnston, K. P. *Chem. Mater.* **2005**, *17*, 6479.
(36) Kang, K.; Gu, G. H.; Kim, D. A.; Park, C. G.; Jo, M.-H. *Chem. Mater.* **2008**, *20*, 6577.

(37) Yong, K.-T.; Sahoo, Y.; Swihart, M. T.; Prasad, P. N. *J. Phys. Chem. C* **2007**, *111*, 2447.
(38) Kamins, T. I.; Williams, R. S.; Basile, D. P.; Hesjedal, T.; Harris, J. S. *J. Appl. Phys.* **2001**, *89*, 1008.
(39) Yutaka, O.; Takeo, S.; Seiji, T.; Atsushi, I.; Yoshihiko, K. *Appl. Phys. Lett.* **2005**, *87*, 043105.
(40) Mathur, S.; Shen, H.; Sivakov, V.; Werner, U. *Chem. Mater.* **2004**, *16*, 2449.
(41) Shah, P. S.; Hanrath, T.; Johnston, K. P.; Korgel, B. A. *J. Phys. Chem. B* **2004**, *108*, 9574.
(42) Kamins, T. I.; Stanley Williams, R.; Hesjedal, T.; Harris, J. S. *Phys. E* **2002**, *13*, 995.
(43) Kamins, T. I.; Williams, R. S.; Chen, Y.; Chang, Y. L.; Chang, Y. A. *Appl. Phys. Lett.* **2000**, *76*, 562.
(44) Kim, B.-S.; Koo, T.-W.; Lee, J.-H.; Kim, D. S.; Jung, Y. C.; Hwang, S. W.; Choi, B. L.; Lee, E. K.; Kim, J. M.; Whang, D. *Nano Lett.* **2009**, *9*, 864.
(45) Persson, M. P.; Lherbier, A. l.; Niquet, Y.-M.; Triozon, F. o.; Roche, S. *Nano Lett.* **2008**, *8*, 4146.